# A prognostic senescence-related long non-coding RNA signature identifies cold and hot tumors of stomach adenocarcinoma

CHENXI HE[1*], FANTING KONG[2*], BAOJUAN HAN[1], LITAO LV[3], XIAOLING WANG[4], XIANGGUANG KONG[1], QINGJIAO ZENG[1] and PEIPEI ZHOU[1]

[1]Department of Gastroenterology, Xingtai People's Hospital, Xingtai, Hebei 054000, P.R. China; [2]Department of Surgical Oncology, Xingtai People's Hospital, Xingtai, Hebei 054000, P.R. China; [3]Department of Gastroenterology, Xingtai Ninth Hospital, Xingtai, Hebei 054000, P.R. China; [4]Medical Research Center, Xingtai Medical College, Xingtai, Hebei 054000, P.R. China

Received December 15, 2025; Accepted April 28, 2026

DOI: 10.3892/ol.2026.15705

**Abstract.** Patients with stomach adenocarcinoma (STAD) have a poor prognosis, and the efficacy of immunotherapy varies widely. The present study aimed to screen effective long non-coding RNAs (lncRNAs) as molecular targets for assessing the prognosis of STAD and guiding precision immunotherapy. A total of five key prognostic senescence-related lncRNAs (SenRLs; AL139147.1, LINC02057, AC093801.1, AL353804.2 and AC005363.2) were screened using bioinformatics methods. A novel validated prognostic risk model was constructed for STAD based on the SenRLs signature. For the training, test and entire set, the 5-year area under the curve values were 0.828, 0.703 and 0.772, respectively. A nomogram combining clinical variables and risk scores effectively predicted overall survival (OS) in patients with STAD. Clinical tissue samples were collected from patients with STAD, and quantitative PCR (qPCR) was employed to assess the tissue expression of SenRLs. The qPCR results showed that the expression of LINC02057, AL139147.1 and AC093801.1 was significantly higher in STAD tissues than in paracancerous tissues. By contrast, the expression of AC005363.2 and AL353804.2 was decreased in STAD tissues. The tissue expression profiles of these lncRNAs were consistent with the bioinformatics findings. The risk groups differed in their immune infiltrating cells, immune checkpoints and susceptibility to chemotherapeutic agents. Following clustering analysis, the two clusters had distinct tumor microenvironment profiles. Notably, based on well-established immunological characteristics, Cluster 2 was identified as representing hot tumors that are presumably more likely to benefit from immunotherapy. The newly developed SenRLs signature can serve as an independent prognostic biological marker of STAD. These SenRLs can effectively distinguish between hot and cold tumors, thereby better facilitating the screening of the beneficiary population for STAD immunotherapy.

*Correspondence to:* Professor Fanting Kong, Department of Surgical Oncology, Xingtai People's Hospital, 818 Xiangdu Road, Xiangdu, Xingtai, Hebei 054000, P.R. China
E-mail: 446984229@163.com

*Contributed equally

*Key words:* senescence, stomach adenocarcinoma, long non-coding RNA, hot tumors, immunotherapy

## Introduction

Gastric cancer is a markedly genetically heterogeneous malignant tumor, which notably affects human life and health. Among all cancer types, gastric cancer ranks fifth in both incidence rate (4.9%) and mortality rate (6.8%) (1). It is reported that >95% of pathological subtypes of gastric cancer are stomach adenocarcinoma (STAD), and numerous patients with gastric cancer have local or remote metastases when they are diagnosed (2). Although the level of early detection and overall therapy continues to improve, the management of progressive gastric cancer remains challenging (3). Its overall efficacy is still unsatisfactory, and new treatments are needed (4).

Immunotherapy has improved the treatment of advanced gastric cancer, but only some patients can benefit from this therapy (5). The biggest challenge with immunotherapy is the wide variation in patient efficacy (6). Some tumor tissues are tolerant or resistant to immunotherapy, leading to the new clinical concepts of cold and hot tumors (7). Tumors characterized by a high density of surrounding T cells and immune cells, which typically respond well to immunotherapy, are classified as 'hot' tumors. By contrast, 'cold' tumors are characterized by sparse immune cell infiltration and poor T cell abundance, and are generally resistant to immunotherapy (8,9). The molecular targets currently used to guide immunotherapy are mainly limited to programmed death ligand-1 (PD-L1) expression levels, microsatellite instability-high and tumor mutational burden (10). These molecular targets, despite some progress, remain controversial (11). STAD tissue stroma is infiltrated by a large number of T lymphocytes, which means that the occurrence of STAD may be more closely related to the tumor microenvironment (TME) (12). Therefore, there is a need to screen for more molecular markers through the comprehensive analysis of the TME to differentiate hot and cold tumors to guide STAD precision immunotherapy.

Cellular senescence is the entry of cells into a state of irreversible proliferative arrest and a specific state of tumor suppression (13). As with other cellular life activities, the onset and progression of cellular senescence are regulated in a sophisticated manner (14). Although the specific mechanisms regulating cellular senescence are not clear, several bioactive substances and their constituent signaling pathways are recognized to participate in the induction, maintenance and termination of senescence, such as p53, p21, p16, p38 and p27 (15). Long non-coding RNAs (lncRNAs) perform numerous functions in life activities, including epigenetics, cell cycle and cellular differentiation (16). LncRNAs are involved in almost all types of diseases, among which the most studied are tumorigenic diseases (17). There is an inextricable link between tumors and senescence (18). Cellular senescence serves a dual role in tumor initiation and progression, acting as either a tumor suppressor or a driver of malignant transformation. Previous studies have shown that certain lncRNAs have been found to appear specifically in senescent cells, interacting with genes or proteins and participating in the regulatory mechanisms of senescence as a node on the senescence signaling pathway (19,20). LncRNA OVAAL, which is notably expressed in ovarian cancer cells, binds PTBP1 competitively with p27 mRNA and inhibits p27 expression, thereby circumventing tumor cell senescence (21). In breast cancer cells, lncRNA PANDAR can regulate the cell cycle G1/S transition by recruiting Bmi1 to the p16 promoter region (22). Recent studies have elucidated that senescence-related lncRNAs (SenRLs) may be utilized as prognostic markers for a variety of cancers, including ovarian cancer (23), colon cancer (24) and head and neck squamous cell carcinoma (25).

A limitation of prior studies is that they have not validated the capacity of corresponding signatures to discriminate immune phenotypes linked to immunotherapeutic benefit. How to precisely identify patients who may derive clinical benefit from such treatments and establish a reliable prognostic stratification system for STAD remains an urgent clinical issue. In the present study, the involvement of SenRLs in STAD prognosis and tumor immune infiltration was investigated using bioinformatic analyses. Notably, the ability of SenRLs to distinguish hot and cold tumor phenotypes was further evaluated, with the ultimate aim of providing a novel reference indicator for precise STAD immunotherapy by identifying immune phenotypes associated with immunotherapy responsiveness. To the best of our knowledge, the signature established in the present study represents the first lncRNA-based prognostic signature in STAD that simultaneously incorporates SenRLs and hot/cold tumor classification.

## Materials and methods

*Datasets and preprocessing*. RNA-sequencing (RNA seq) datasets, metadata and clinical information for 375 STAD samples and 32 control samples were obtained from The Cancer Genome Atlas (TCGA) database (https://portal.gdc.cancer.gov/). The RNA-seq dataset and metadata files were processed using the Perl script (version 1.7.8) (https://bioperl.org/) to obtain the gene expression matrix, followed by ID transformation to obtain the corresponding gene names. STAD samples with indeterminate clinical stages and survival time <30 days were excluded.

*Obtaining SenRLs*. Human senescence genes were obtained from the Human Ageing Genomic Resources database (https://genomics.senescence.info/) (Table SI). To create the senescent gene expression matrix file, the limma R package (version 3.56.0) (https://bioconductor.org/packages/release/bioc/html/limma.html) was used to determine the intersection of senescent genes with the gene expression matrix. Pearson correlation analysis was applied to analyze the co-expression of lncRNAs and senescence-related genes. The expression of lncRNAs and senescence-related genes was defined as function variables, and the correlation between them was tested to obtain correlation coefficients and P-values. The SenRLs were extracted with |Correlation Coefficient|>0.4 as well as P<0.001 (26). Cytoscape (version 3.6.1) (https://cytoscape.org/) was used to visualize the coexpression network.

*SenRLs survival data acquisition*. The sample name, survival time and survival status were the only information kept in the clinical data of STAD cases that were obtained from the TCGA database. The survival times were sorted in ascending order to remove samples with unclear survival times. Next, survival status was sorted in ascending order, and samples with unclear survival status were deleted. The processed survival information was merged with the SenRLs expression data to produce SenRLs survival data for STAD for subsequent analysis.

*Identification and verification of risk models*. Using R software packages (version 4.3.1; RStudio, Inc.), patients within the SenRLs survival data file were split into training and test sets at random. Univariate Cox regression was performed to screen STAD prognostic SenRLs based on P<0.05. Kaplan-Meier analyses were also conducted requiring KM <0.05 and plotted forest plots using the survival (version 3.4-0; https://cran.r-project.org/package=survival) and survminer (version 0.4.9; https://cran.r-project.org/package=survminer) R packages. Next, these SenRLs were further included in a multivariate Cox regression to get the key lncRNAs applied to create the prognostic risk model and to get the regression coefficients. Risk scores were calculated utilizing the regression coefficients and expression values of SenRLs. The median risk score was used to divide patients into different risk groups. The Sankey diagrams were made using the R tool ggalluvial (version 0.12.5) (https://cran.r-project.org/package=ggalluvial). Survival analysis was then carried out using the survminer (version 0.4.9; https://cran.r-project.org/package=survminer) R package. To examine the survival disparities between the two groups, Kaplan-Meier survival curves were charted. Receiver operating characteristic (ROC) curves were produced using timeROC (version 0.4; https://cran.r-project.org/package=timeROC), and area under the curve (AUC) values were calculated to compare the role of different factors in predicting outcomes. Scatterplot3D (version 0.3-44; https://cran.r-project.org/package=scatterplot3d) R package was applied to create principal component analysis (PCA) plots. Univariate and multivariate Cox regression analyses were carried out on risk value as well as clinicopathological

Table I. Reverse transcription-quantitative PCR primer details.

| Primer | Sequence | Tm, ˚C | Product size, bp |
|---|---|---|---|
| AL139147.1-F | CTCTACCAATGTGATGCGAATGA | 59.40 | 193 |
| AL139147.1-R | GGCTCTCTGTTTGTCTGTTATTTGT | 60.30 | |
| LINC02057-F | TAAGGCAGGCTTCGGAAATGAG | 61.21 | 129 |
| LINC02057-R | GTGAATGATGTCCAGCTTTTTGGTC | 61.62 | |
| AL353804.2-F | GGAATAATGTGAAAACACTTGAGCA | 59.08 | 177 |
| AL353804.2-R | CTCTAATAGTAAGAAAACTGAGTCCTG | 57.73 | |
| AC005363.2-F | CATTTGTAGCCAGCGTTTACTCCT | 60.73 | 134 |
| AC005363.2-R | TTATTTATCAAGAGCCACACTGCGA | 60.86 | |
| AC093801.1-F | AAGCTCCCTACAGCATCCAC | 59.46 | 102 |
| AC093801.1-R | GCCACACATTGTCTCATGTTCATAC | 60.67 | |
| ACTB-F | CAGTCGGTTGGAGCGAGCAT | 62.84 | 135 |
| ACTB-R | TGGCTTTTAGGATGGCAAGGGAC | 63.03 | |
| GAPDH-F | AACAGCCTCAAGATCATCAGCAA | 61.16 | 104 |
| GAPDH-R | GTCATGAGTCCTTCCACGATACC | 61.08 | |

Tm, melting temperature; F, forward; R, reverse.

information to clarify whether risk values were independent prognostic indicators.

*Nomogram and gene set enrichment analysis (GSEA).* With the rms (version 6.7-1; https://cran.r-project.org/package=rms) R package, a clinically useful nomogram was developed and validated. Calibration curves were applied to demonstrate the predictive power of the nomogram. To further investigate the biological functions and pathways associated with the prognostic SenRLs signature, Gene Ontology (GO) and Kyoto Encyclopedia of Genes and Genomes (KEGG) enrichment analyses were performed using the GSEA software (version 4.1.0; https://www.gsea-msigdb.org/gsea/index.jsp). The analysis was conducted with the following parameters: the phenotypic file was set to h_vs._1, the permutation type was adjusted to phenotype, the number of simulations was fixed to 1,000 and the plot graphs for the top sets of each phenotype were set to 5. Significantly enriched pathways were identified based on a nominal P-value <0.05 and a false discovery rate (FDR) <0.25.

*Reverse transcription-quantitative PCR (RT-qPCR) assay of tissue specimens.* STAD tissue specimens and paired paraneoplastic tissue specimens were acquired from 15 patients treated at Xingtai People's Hospital (Xingtai, China) and identified as STAD by postoperative pathology between March 2025 and September 2025. All included STAD cases were exclusively identified as the intestinal type according to Lauren's classification (1965) (27), with pathological diagnoses established in accordance with the WHO Classification of Tumours of the Digestive System (28). To ensure diagnostic accuracy, the histological subtyping and final diagnosis were independently reviewed and confirmed by two senior pathologists from Xingtai People's Hospital. The patients with STAD included 8 males and 7 females, aged 41 to 68 years. All patients were strictly screened, with no history of other malignant tumors and no prior radiotherapy, chemotherapy, targeted therapy or immunotherapy. The Xingtai People's Hospital Ethics Committee approved the study (approval no. 2025-048). Written informed consent was voluntarily obtained from each patient or their authorized family member. The present study was conducted in accordance with The Declaration of Helsinki. Tissue samples were collected immediately after the operation, quickly frozen with liquid nitrogen and then carefully transported and kept in a refrigerator at -80˚C.

Total RNA was extracted using TRIzol® reagent (Invitrogen; Thermo Fisher Scientific, Inc.) according to the manufacturer's protocol. First-strand cDNA was synthesized using the Takara PrimeScript RT Kit (Takara Bio, Inc.) following the manufacturer's instructions. RT-qPCR detection employed the SYBR Premix Ex Taq™ Kit (Takara Bio, Inc.), strictly adhering to the manufacturer's operating procedures. The primers used in this procedure were synthesized by Sangon Biotechnology Co., Ltd., and Table I lists the primer sequences. The following are the thermal cycling conditions employed for qPCR: An initial denaturation step at 95˚C for 5 min; followed by 40 cycles, each consisting of 5 sec denaturation at 95˚C, 30 sec annealing at 60˚C and 30 sec extension at 72˚C; concluding with a final extension step at 72˚C for 2 min. The relative amounts of genes were analyzed by $2^{-\Delta\Delta Cq}$ (29) with GAPDH and ACTB as internal reference. A paired t-test was employed to compare the expression levels of these SenRLs between STAD tissues and paired paracancerous tissues.

*Immune cell infiltration and drug sensitivity analysis.* The immune infiltration landscape of each STAD sample was quantified utilizing CIBERSORT (version 1.03) (https://cibersort.stanford.edu/). For immune cell analysis and visualization using bubble plots the following were utilized: XCELL, TIMER, QUANTISEQ, MCPCOUNTER, EPIC, CIBERSORT-ABS and CIBERSORT on TIMER2.0 (http://timer.cistrome.org/). Following this, the limma,

ggplot2 (version 3.4.2) (https://ggplot2.tidyverse.org), ggpubr (version 0.6.0; https://rpkgs.datanovia.com/ggpubr/) and ggextra (version 0.10.1; https://github.com/daattali/ggExtra) R packages were utilized to determine the association between the immune infiltration and the model. According to the Genomics of Drug Sensitivity in Cancer (https://www.cancerrxgene.org/), the half-maximal inhibitory concentration (IC50) differences across groups were compared, and the results are presented as box plots.

*Cluster analysis based on SenRLs*. Using the ConsensusClusterPlus (version 1.66.0; https://bioconductor.org/packages/ConsensusClusterPlus/) in R software, consensus clustering was carried out utilizing the expression of key prognostic SenRLs. The pheatmap (version 1.0.12; https://cran.r-project.org/package=pheatmap) R package was used to build heatmaps for clustering. PCA and t-distributed stochastic neighbor embedding (t-SNE) analysis were carried out using the Rtsne (version 0.16; https://cran.r-project.org/package=Rtsne) R package. Utilizing the survival (version 3.5-7; https://cran.r-project.org/package=survival) and survminer R packages, survival analysis was performed for clusters, and survival curves were plotted. Utilizing single sample GSEA with the GSVA (version 1.48.3; https://bioconductor.org/packages/GSVA/) R package, enrichment scores of immunological pathways were calculated. The TME of the two clusters was scored and compared using the estimate (version 1.8.2; https://bioconductor.org/packages/estimate/), limma and BiocManager (version 1.30.22; https://cran.r-project.org/package=BiocManager) R packages. Immunocheckpoint gene analysis was performed for both clusters using ggplot2 and ggpubr R packages.

*Multi-model machine learning validation and Shapley additive exPlanations (SHAP) analysis*. To further validate the reliability and interpretability of the established prognostic SenRLs signature, multi-model machine learning and SHAP analysis were performed. A total of four distinct classification models were constructed: Random Forest (RF), Gradient Boosting Machine (GBM), Support Vector Machine (SVM) and K-Nearest Neighbors (KNN). Subsequently, SHAP analysis was conducted using the SHAP Python package (version 0.44.0; https://github.com/slundberg/shap).

*Statistical analysis*. Survival analyses utilizing the Kaplan-Meier method were performed for different groups or clusters. A weighted test (Renyi test) was used to compare the survival differences between the high and low lncRNAs expression groups. Clinical information was analyzed through GraphPad Prism (version 8.0; Dotmatics) using the $\chi^2$ test. Statistical analysis was performed utilizing R software (version 4.3.1; RStudio, Inc.). $P<0.05$ was considered to indicate a statistically significant difference.

## Results

*STAD prognostic SenRLs screening*. Co-expression analysis among cellular senescence-associated genes and lncRNAs revealed 1,619 SenRLs, visualized as a network (Fig. 1A). The expression differences of SenRLs in STAD and normal samples were examined [|log2 fold change|>1 and false discovery rate (FDR)<0.05]. The findings demonstrated that there were variations in the expression levels of 789 SenRLs, with 192 lncRNAs exhibiting low expression and 597 lncRNAs exhibiting high expression. The results were visualized with a volcano plot (Fig. 1B). Heatmaps were constructed to demonstrate the expression density of 100 of these SenRLs (Fig. 1C). The survival of patients with STAD was notably correlated with 11 SenRLs, according to univariate Cox regressions and Kaplan-Meier analysis ($P<0.05$; KM<0.05; Table SII). A total of six of these were protective lncRNAs [hazard ratio (HR)<1], and the other five were risk-related lncRNAs (HR>1) (Fig. 1D). Heatmaps were used to display the expression of 11 SenRLs in patients with STAD and normal samples (Fig. 1E).

*Development and assessment of STAD prognostic models*. A total of five key prognostic SenRLs (AL139147.1, LINC02057, AC093801.1, AL353804.2 and AC005363.2) were screened by multivariate Cox regression analysis ($P<0.05$; Table SIII). AL353804.2 and AC005363.2 were protective lncRNAs, and the remaining three were risk-related lncRNAs (Fig. 2A). Kaplan-Meier survival curves were plotted, utilizing the expression of each of these five lncRNAs. The Renyi test was employed to compare survival differences between high- and low-expression groups, given its robustness in handling survival curve crossovers. The high expression group of AL139147.1, LINC02057 and AC093801.1 showed poorer overall survival (OS) ($P<0.05$), as demonstrated in Fig. 2B-D. The AL353804.2 and AC005363.2 high-expression groups had a prolonged survival time ($P<0.05$; Fig. 2E and F).

Based on these five lncRNAs, the prognostic SenRLs signature was established. Risk score=(coef 1.81069714813647 x expr AL139147.1) + (coef 0.950768101588694 x expr LINC02057) + (coef 1.17094750602435 x expr AC093801.1) + (coef-1.06513974991373 x expr AL353804.2) + (coef-1.25744132430942 x expr AC005363.2). coef denotes the regression coefficient derived from multivariate Cox regression analysis, and expr indicates the expression level of each SenRL. The allocation of risk score distribution, survival status and expression of the five lncRNAs were determined in the two groups of patients from the TCGA dataset (Fig. 3A-I). The results indicate that the risk score determines the prognosis of STAD, and patients with high-risk values had worse survival status. In the high-risk group, the expression of LINC02057, AL139147.1 and AC093801.1 was notably greater, while the expression of AC005363.2 and AL353804.2 was decreased. Kaplan-Meier survival analysis was performed in the present study for the training set, test set and whole set, respectively (Fig. 3J-L). The results all displayed that the OS of patients in the high-risk group was significantly lower ($P<0.05$). For the training set, test set and whole set, the 5-year AUC values were 0.828, 0.703 and 0.772, respectively (Fig. 3M-O). The 5-year ROC of the SenRLs signature had notable predictive efficacy.

*Verification of the SenRLs signature*. As demonstrated in the univariate Cox regression analysis (Fig. 4A), the risk score was significantly associated with patient prognosis ($P<0.001$). Furthermore, the multivariate Cox regression analysis (Fig. 4B), which adjusted for other clinical covariates, confirmed that the risk score remained a significant prognostic indicator

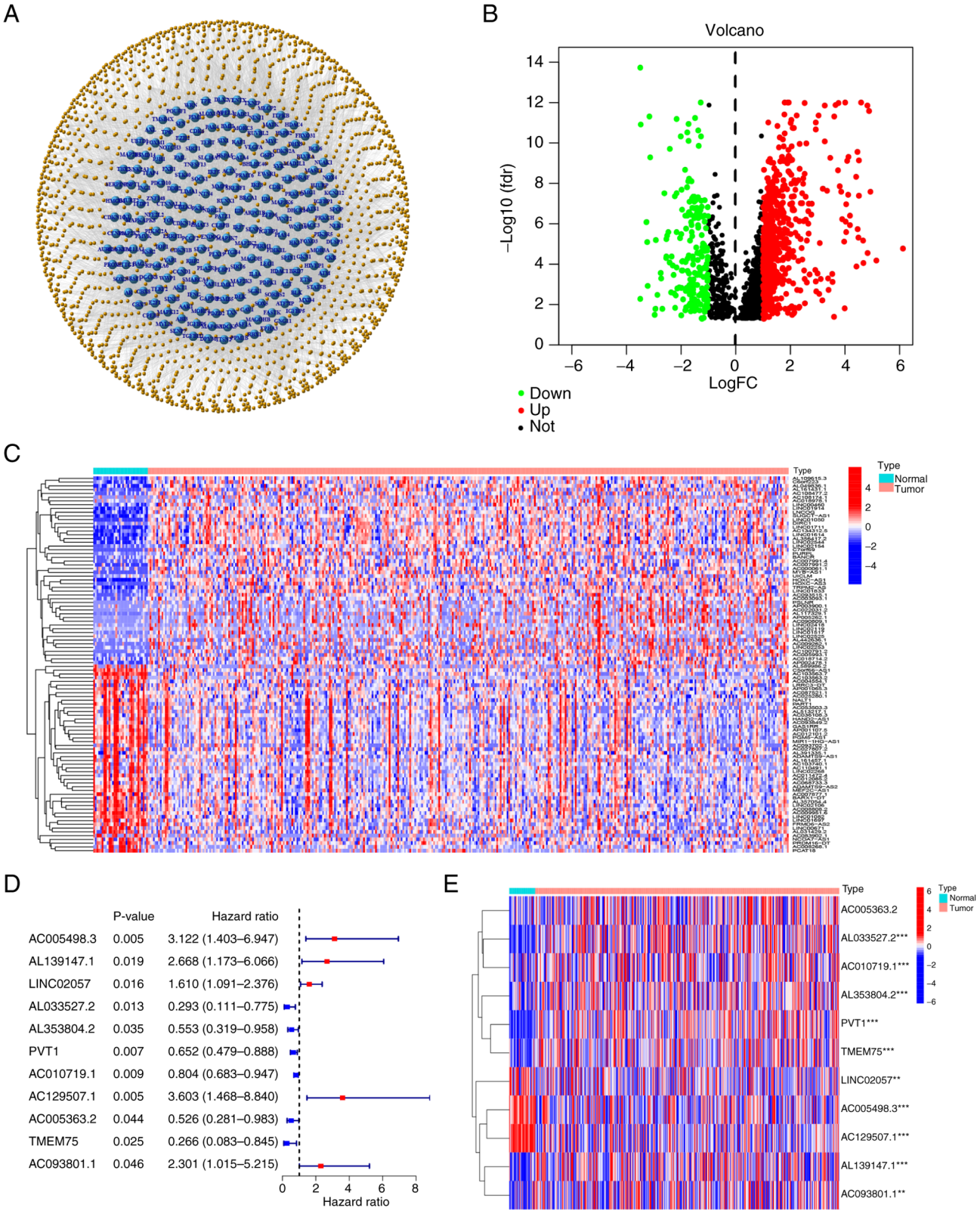


Figure 1. Identification of SenRLs. (A) Network diagram between senescence-related mRNAs and lncRNAs. Yellow dots represent lncRNAs, and blue dots represent mRNAs. (B) Volcano plot of differential expression of SenRLs. Red dots indicate high expression, and green dots indicate low expression. (C) Expression heatmap of 100 SenRLs. The horizontal coordinates represent samples, and the vertical coordinates represent lncRNAs. (D) Forest plot of 11 prognostic SenRLs. (E) 11 SenRLs' expression in samples is shown in a heatmap. lncRNA, long non-coding RNA; SenRLs, senescence-related lncRNAs; FC, fold change; fdr, false discovery rate.

(P<0.001). These results suggest that the SenRLs signature is an independent factor affecting patient prognosis. The AUC of the risk score was 0.752, which was greater than that of the other medical factors (Fig. 4C), indicating the notable accuracy of the model. Next, PCA was performed based on all the SenRLs identified via univariate Cox regression and the 5 key

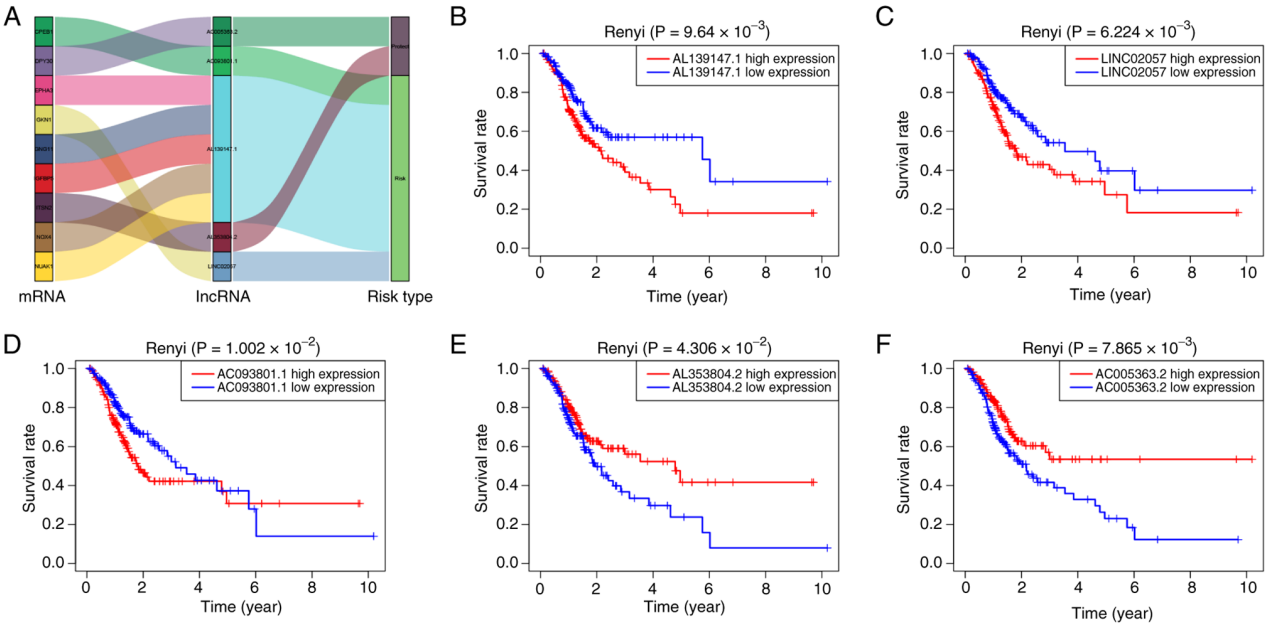


Figure 2. Sankey diagrams and Kaplan-Meier survival curves. (A) The relationship between 5 senescence-related lncRNAs, mRNAs and risk types. Kaplan-Meier survival curves according to five lncRNAs expression levels: (B) AL139147.1, (C) LINC02057, (D) AC093801.1, (E) AL353804.2 and (F) AC005363.2. lncRNA, long non-coding RNA.

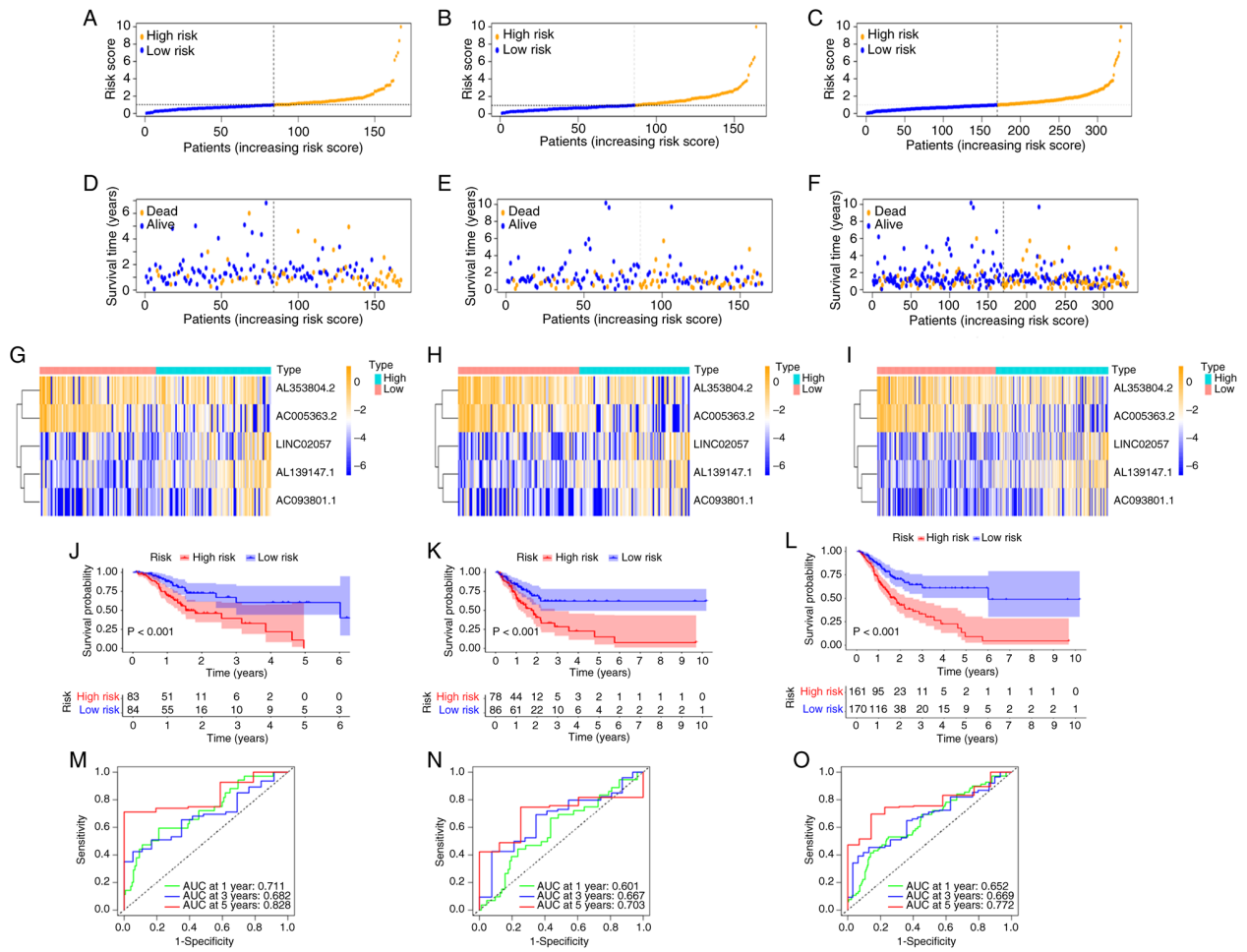


Figure 3. Prognostic value of the SenRLs model. (A-C) Risk score curves for the (A) training set, (B) test set and (C) whole set. (D-F) Survival status for the (D) training set, (E) test set and (F) whole set. The blue and yellow dots symbolize life and death, respectively. (G-I) Expression of five prognostic SenRLs on a heatmap for the (G) training set, (H) test set and (I) whole set. (J-L) Kaplan-Meier survival curves in risk groups for the (J) training set, (K) test set and (L) whole set. (M-O) Receiver operating characteristic curves for different times for the (M) training set, (N) test set and (O) whole set. (5-year AUC >0.7). lncRNA, long non-coding RNA; SenRLs, senescence-related lncRNAs; AUC, area under the curve.

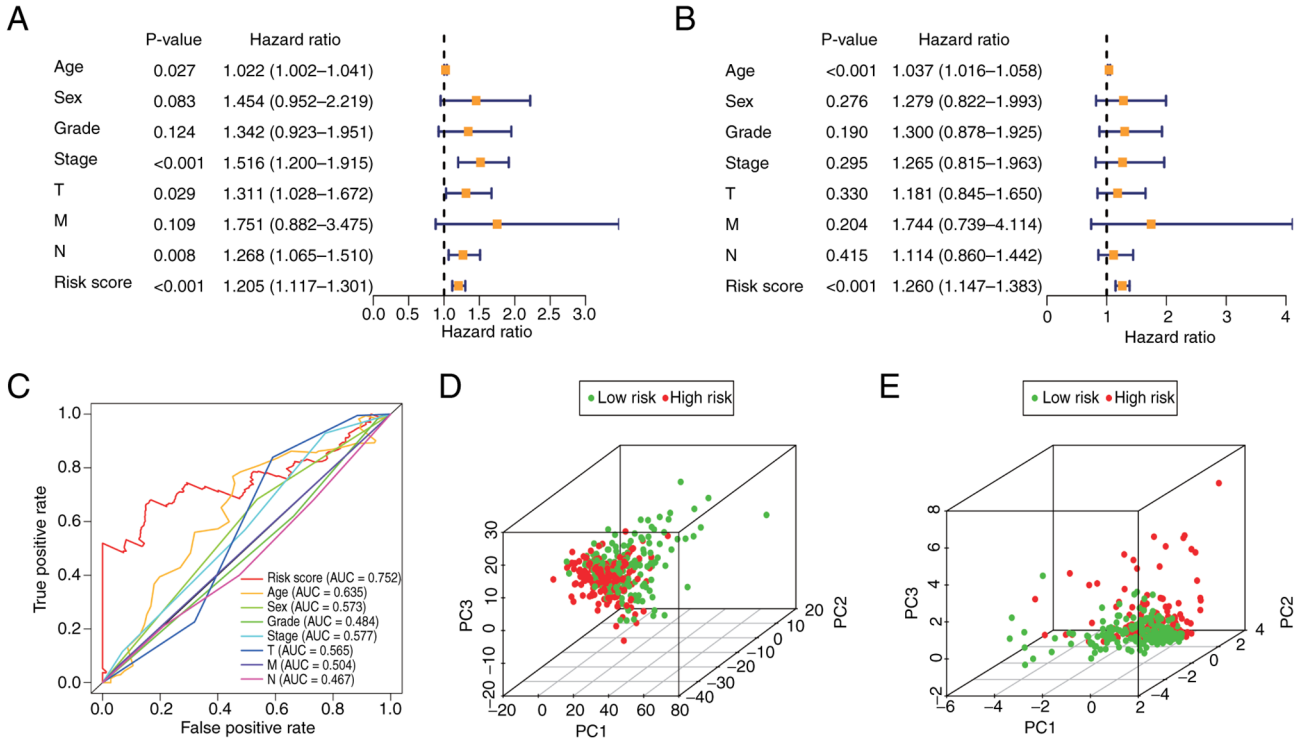


Figure 4. SenRLs signature is a prognostic marker of stomach adenocarcinoma. (A) Univariate and (B) multivariate Cox regression analysis. (C) Receiver operating characteristic curves of risk score and clinicopathological factors. PC analysis based on (D) SenRLs and (E) 5 key prognostic SenRLs. lncRNA, long non-coding RNA; SenRLs, senescence-related lncRNAs; PC, principal component; AUC, area under the curve. T, tumor invasion depth; N, regional lymph node metastasis; M, distant metastasis.

prognostic SenRLs, respectively. As shown in Fig. 4D, all the SenRLs could not effectively discriminate between the high and low-risk groups; however, based on the key prognostic SenRLs signature, there was a significant distribution distinction between the two groups (Fig. 4E); therefore, the PCA findings further support the accuracy of the model.

*Relationship between SenRLs signature and clinicopathological factors*. The clinical indicators (including age, gender, tumor grade, and TNM stage) were subdivided, and Kaplan-Meier survival curves were plotted for the subgroups stratified by these clinical indicators. The model was found to apply to clinical factors such as age, sex, grade 2, grade 3, T3 and T4 staging (Fig. 5). However, there was no statistical difference in OS in some subtypes, such as grade 1, T1 and T2. This may be related to the overly refined subgroup typology and the small number of patient cases in the subgroup. Next, the relationship between risk values and clinicopathological parameters was analyzed to learn more about the function of the SenRLs signature in the development of STAD. Patients who developed distant metastases had significantly higher risk values than those without distant metastases (P<0.001; Fig. 6A). In addition, the survival status was lower for patients with STAD with high-risk values (P<0.001; Fig. 6B). Risk values in STAD are notably linked to distant metastases and death, and the SenRLs signature may be involved in STAD disease progression.

*Establishment of a nomogram*. To achieve individualized prognosis prediction of patients with STAD, a nomogram was constructed combining risk score and clinical variables (Fig. 7A). There was a high agreement between the expected and actual observed values, as demonstrated by the calibration curves, which revealed that the predicted curves for survival were all around the standard curves (Fig. 7B-D). Therefore, the nomogram combining medical factors and risk score is effective in forecasting patient OS.

*RT-qPCR to confirm lncRNAs expression*. The present study quantified the expression of five key prognostic lncRNAs using RT-qPCR in 15 pairs of STAD tissue specimens and paracancerous tissue specimens in order to further test the viability of the SenRLs signature. The results are shown in Fig. 8, and the expression of LINC02057, AL139147.1 and AC093801.1 was significantly greater in STAD than in paracancerous tissues. The expression of AC005363.2 and AL353804.2 was significantly decreased in STAD tissues. The tissue expression profiles of these lncRNAs are consistent with the bioinformatics findings, thus confirming the reliability and accuracy of the above analysis results.

*GSEA*. Next the specific signaling pathways involved in prognostic SenRLs was investigated by enrichment analysis. Through GO analysis, it could be seen that the signaling pathways, such as 'collagen-containing extracellular matrix', 'peptide receptor activity' and 'glycosaminoglycan binding', were enriched in the high-risk group. The low-risk group was enriched for signaling pathways such as 'mRNA splice site selection', 'mRNA 5 splice site recognition' and 'spliceosomal complex assembly' (P<0.05; FDR<0.25; Fig. 9A).

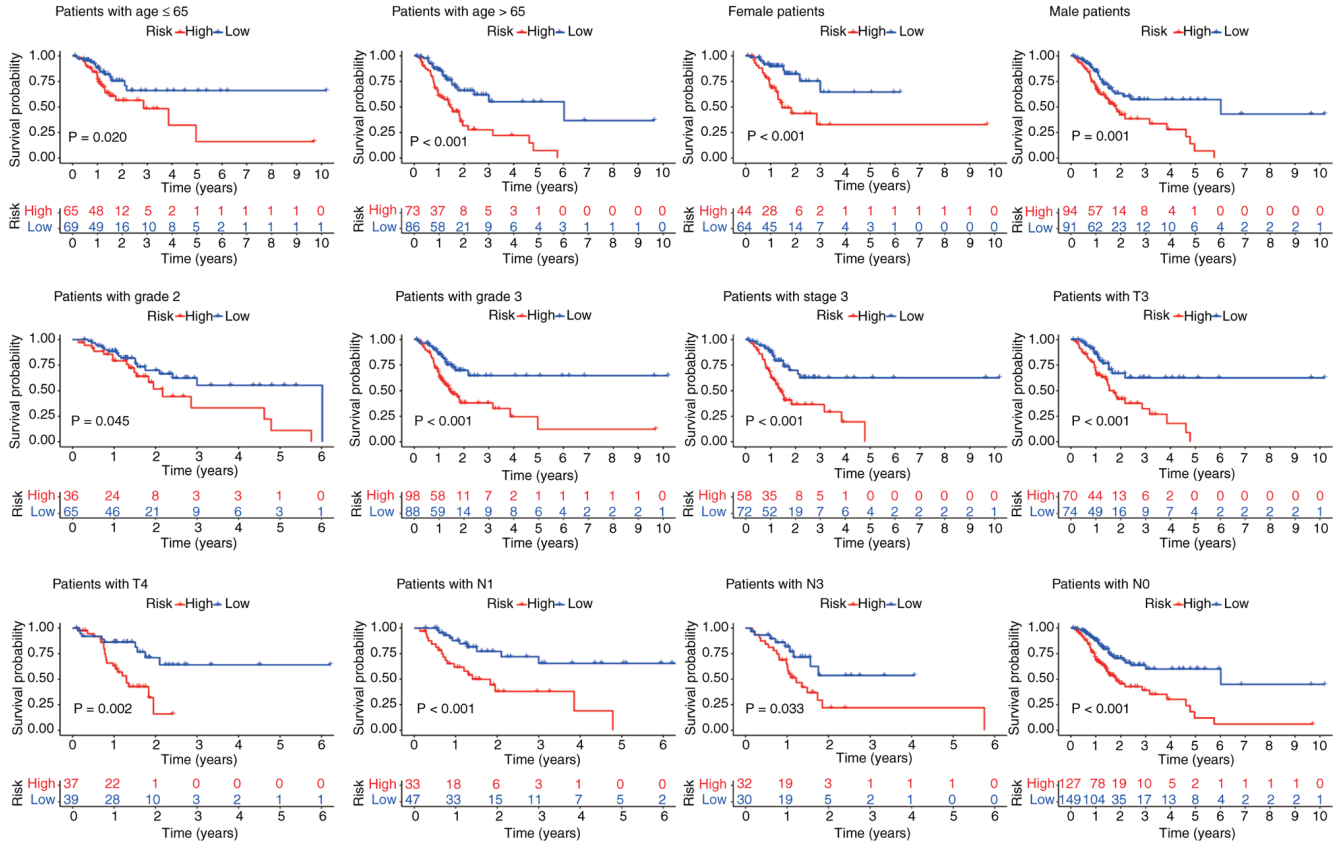


Figure 5. Survival curves in different clinical subgroups.

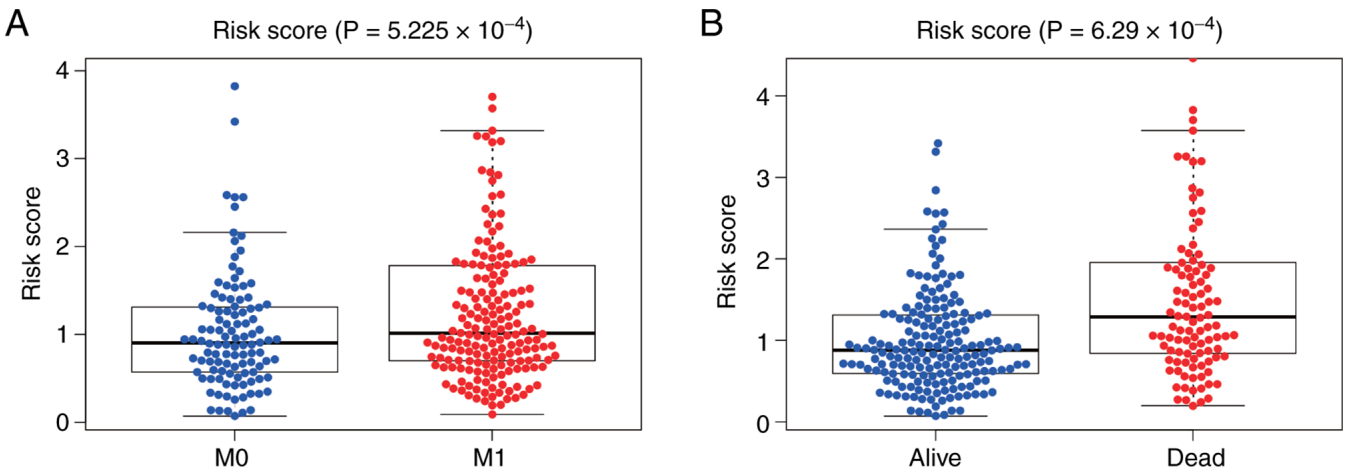


Figure 6. Relationship between risk values and clinicopathological parameters. Association of risk score with (A) distant metastasis and (B) survival status.

Further analysis by KEGG showed that signaling pathways such as the 'intestinal immune network of IgA production', 'cytokine-cytokine receptor interaction' and 'cell adhesion molecules cams' were enriched in the high-risk group (P<0.05; FDR<0.25; Fig. 9B). No significant differences in KEGG gene concentration were observed in the low-risk group. The immune response-related signaling pathways were markedly enriched in the high-risk group, suggesting that prognostic SenRLs may influence STAD development through immune pathways. Next, immunological analysis was performed in the model.

*Immunoscape and treatment*. The relative proportions of 22 immunological infiltrating cells were analyzed using CIBERSORT, and the results were displayed as a bar chart (Fig. S1). A correlation analysis of immune cells was performed using seven working platforms, including XCELL, TIMER and QUANTISEQ. As shown in the bubble plot in Fig. 10A, the high-risk group had more immune cell infiltration, such as Monocyte, Myeloid dendritic cell, B cell naive, T cell CD8+, Macrophage, NK cell and B cell (P<0.05, Table SIV). The study further analyzed the correlation between risk score and immune cell infiltration. It showed that the risk score was

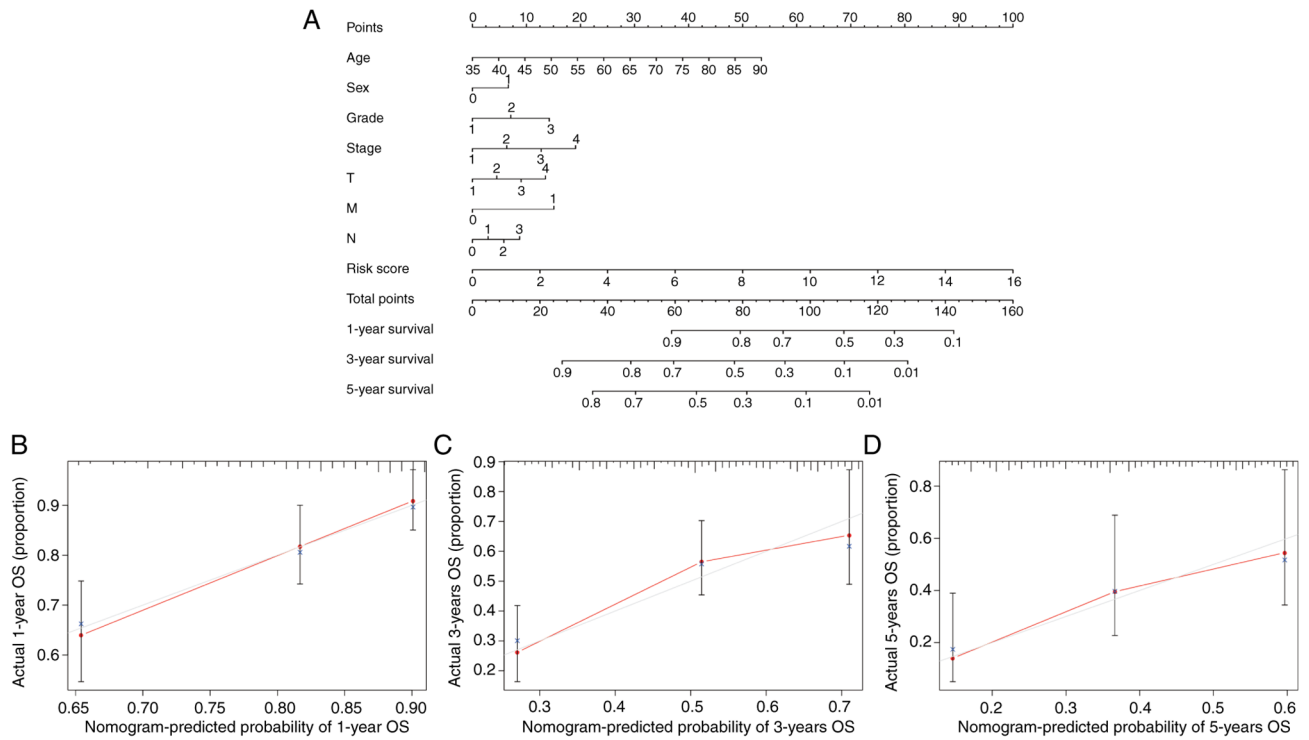


Figure 7. Nomogram of clinical applicability. (A) Nomogram for personalized prediction of OS in patients with stomach adenocarcinoma. Calibration curves for (B) 1 year, (C) 3 years and (D) 5 years. OS, overall survival.

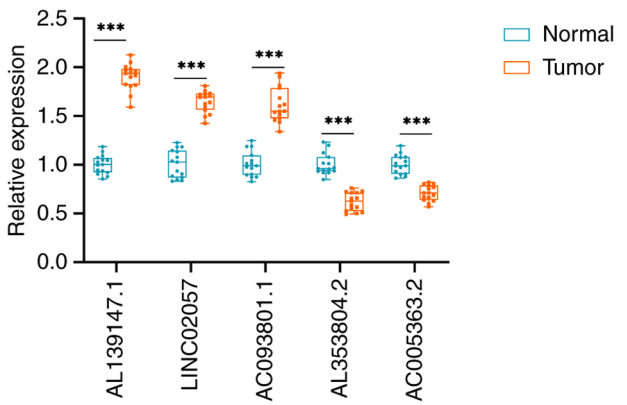


Figure 8. Reverse transcription-quantitative PCR was utilized to evaluate the expression of five senescence-related long non-coding RNAs in tissues. ***P<0.001.

positively correlated with most immune cell infiltration, such as dendritic cells activated, mast cells resting, monocytes and neutrophils (P<0.05; Fig. 10B). Therefore, this demonstrated that the SenRLs signature-based risk score is effective in distinguishing different features of immune cells in STAD.

Immune checkpoint inhibitor (ICI) selectively enhances host immune response to malignancies by modulating the TME (30). It was observed how immunological checkpoints were expressed in patients with STAD. The high-risk group had high expression levels of the majority of immune checkpoint genes, including *CD40LG*, *CD200* and *ICOSLG* (P<0.05; Fig. 10C). This implies that patients with STAD can be grouped by the SenRLs risk patterns to select appropriate checkpoint inhibitors for them. The IC50 values for the chemotherapeutic medications methotrexate and mitomycin C differed significantly between the two groups, with the high-risk group having higher IC50 values (P<0.01; Fig. 10D and E). Therefore, the SenRLs signature could be used as a potential predictor of drug sensitivity for oncology treatment.

*Hot and cold tumor classification in STAD.* Clustering analysis of STAD samples was performed depending on the SenRLs signature to improve the characterization of the subtypes of cold and hot tumors in the samples. Combining the matrix clustering heatmap, cumulative distribution function (CDF) and area change beneath the CDF plot, the sub-groups at K=2 (the highest intra-group correlation) were selected as the clustering result in this study (Fig. 11A and B and Fig. S2). The samples were divided into 2 groups, named Cluster 1 and Cluster 2, respectively. Both t-SNE and PCA showed that the above division could better classify the samples into two clusters (Fig. 11C and D). The OS of the two clusters was compared, and the OS of Cluster 2 was superior to Cluster 1, but no significant difference was found (P=0.188; Fig. S3). Cluster subtyping cannot be used as a prognostic indicator, and the risk score of the SenRLs signature remains the main OS predictor. In addition, charts were developed to understand the correlation of clustering with risk groups, and according to Fig. 11E, Cluster 1 is linked to high risk, whereas Cluster 2 is linked to low risk.

The examination of the various platforms showed discrimination in the immune cell infiltration of the clusters (P<0.01; Table SV). The enrichment scores for the immunological pathways and immune cells were calculated. These findings revealed that a variety of immune cells, such as regulatory

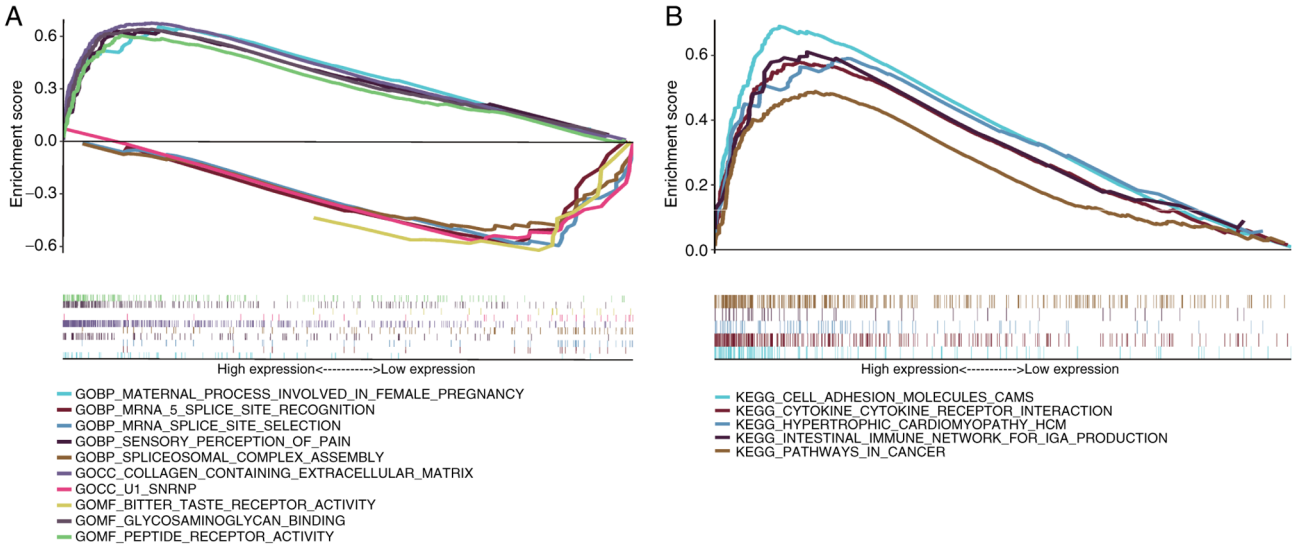


Figure 9. First 5 significantly enriched pathways according to gene set enrichment analysis. (A) GO pathway. (B) KEGG analysis. GO, gene ontology; KEGG, Kyoto Encyclopedia of Genes and Genomes; BP, biological process; CC, cell component; MF, molecular function.

T cells (Treg), T follicular helper cells (Tfh), T helper (Th)1 cells, dendritic cells (DCs), immature DCs (iDCs), plasmacytoid DCs (pDCs) and CD8+ T cells, had elevated enrichment scores in Cluster 2 (P<0.05; Fig. 11F). T cell co-stimulation and other immune function enrichment fractions were notably greater in Cluster 2 (P<0.01; Fig. 11G), suggesting that Cluster 2 is more important in immune cell function regulation. Compared with Cluster 1, Cluster 2 had significantly greater immune, stromal and estimate scores (P<0.01; Fig. 11H-J). The two clusters have different TME, and immunotherapy is dependent on TME (31). Most of the immune checkpoint genes, including *PDCD1LG2* (also called programmed death ligand-2, *PD-L2*), *HAVCR2* (also called T-cell Immunoglobulin and Mucin Domain-containing Protein 3, *TIM3*) and *CD274* (also called *PD-L1*), were upregulated in Cluster 2 (P<0.05; Fig. 11K). A tumor is defined as 'hot' if it contains abundant tumor-reactive immune cells, displays an active immune microenvironment and exhibits high expression of immune checkpoints (8,9). In the present study, Cluster 2 showed marked immune cell infiltration, a more active TME (with greater enrichment of immune function-related pathways and higher immune/stromal/estimate scores), and elevated immune checkpoint expression. Based on these canonical immunological features, Cluster 2 is likely to be more responsive to immunotherapy and can therefore be classified as a hot tumor. By contrast, Cluster 1 exhibited immunotherapy resistance and can be categorized as a cold tumor.

*Multi-model validation and SHAP analysis*. To verify the robustness of the model, cross-validation was performed using four different algorithms, and all AUC values were >0.7. The RF and GBM models achieved the highest AUC of 0.849, indicating excellent and stable predictive performance (Fig. S4A). The mean absolute SHAP value of each SenRL served as a metric for its relative importance; AL139147.1 exhibited the highest value (0.0412) (Fig. S4B). This ranking of importance was consistent with the results of the multivariate Cox regression, in which AL139147.1 showed the highest coefficient (1.811), validating the logical consistency of the signature. Additionally, the SHAP waterfall plot visualized the additive prediction process (Fig. S4C). Starting from a base value of $E[f(x)]$=0.913, the final prediction reached $f(x)$=0.978. AL139147.1, AC093801.1 and LINC02057 emerged as positive contributors, whereas AC005363.2 and AL353804.2 contributed negatively, a pattern consistent with the risk model. Collectively, these data confirm that the model relies on distinct, biologically plausible feature contributions rather than randomness, substantiating its validity and interpretability.

## Discussion

Cellular senescence is the basic unit of senescence in the whole organism, and senescent cells contribute to the gradual aging of the organism through the release of inflammatory signals (32). At the same time, cellular senescence can eliminate abnormal cells and prevent the further release of tissue-damaging factors from degenerated cells. This is an important mechanism by which the organism performs self-clearance and maintains a healthy microenvironment and immune response (32). LncRNAs have a notable role in the regulatory mechanism of cellular senescence. LncRNA Pvt1b is a mediator of p53-dependent growth arrest, and Pvt1b expression is cis-regulated by p53, which causes lung adenocarcinoma and sarcoma cells to undergo senescence (33).

Numerous senescence-related gene signatures have been established to predict the prognosis of patients with malignant tumors, including gastric cancer (34), colon adenocarcinoma (35) and prostate cancer (36). However, most previous studies have been mainly based on mRNA expression profiles. Given the marked regulatory roles of lncRNAs in tumor cell senescence, the development of a SenRLs prognostic signature for STAD remains warranted. In the present study, a STAD prognostic risk model was built utilizing five SenRLs (AL139147.1, LINC02057, AC093801.1, AL353804.2 and AC005363.2). The ROC curves indicated that the SenRLs signature had an excellent predictive

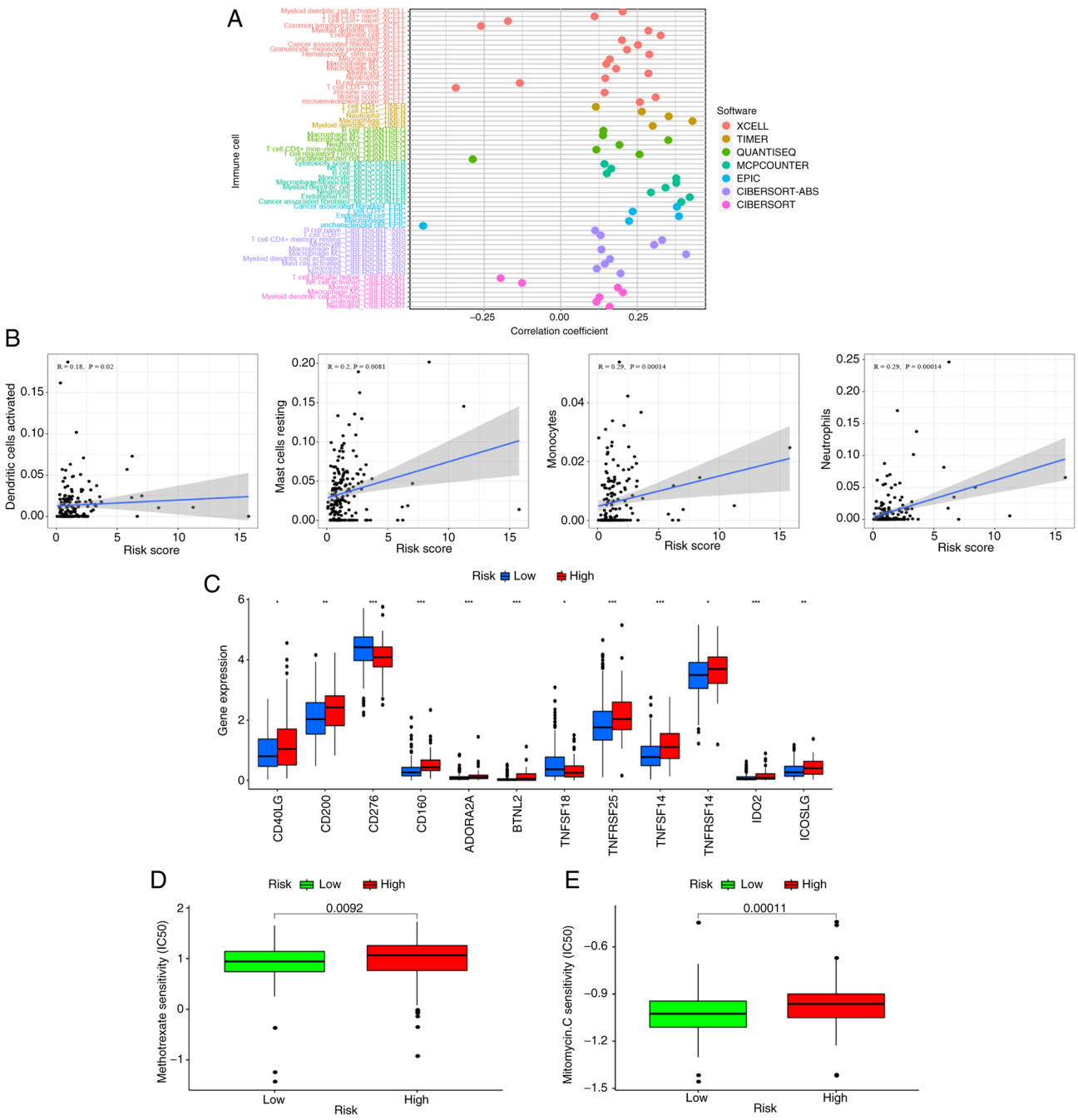


Figure 10. Immunocorrelation assessment and medication sensitivity of senescence-related long non-coding RNAs characteristics. (A) Immune cell bubble map of the risk model. (B) Scatter plot showing the relationship between immune cells and risk values. (C) Variations between the two groups in immune checkpoint gene expression. Sensitivities to (D) methotrexate and (E) mitomycin C. $^{*}$P<0.05, $^{**}$P<0.01, $^{***}$P<0.001.

performance for 5-year OS in patients with STAD. SenRLs performed better as an independent prognostic indicator than traditional clinicopathological factors. Furthermore, the risk values for the prognostic prediction model were shown to be linked to metastasis stage and survival status, suggesting that the SenRLs signature is linked to STAD progression. Using RT-qPCR, the expression of SenRLs was validated, and the outcomes further supported the validity of the bioinformatics analysis findings. The present study constructed a nomogram by combining risk score, age and TNM staging in order to achieve individualized prediction of OS in patients with STAD. The newly developed nomogram can effectively predict the risk of patient death and is expected to assist in the development of clinical treatment strategies.

The malignant phenotype of tumors is determined not only by tumor cell-intrinsic activity but also by immune cells recruited and activated in the tumor-associated microenvironment (37). In the present study, GSEA demonstrated that the SenRLs signature is mainly involved in immune response-associated pathways. Next, the link between the SenRLs signature and TME was further investigated. The high-risk score was significantly correlated with the majority of immune cells. Furthermore, it was noted that the infiltration abundance of neutrophils, activated dendritic cells, resting

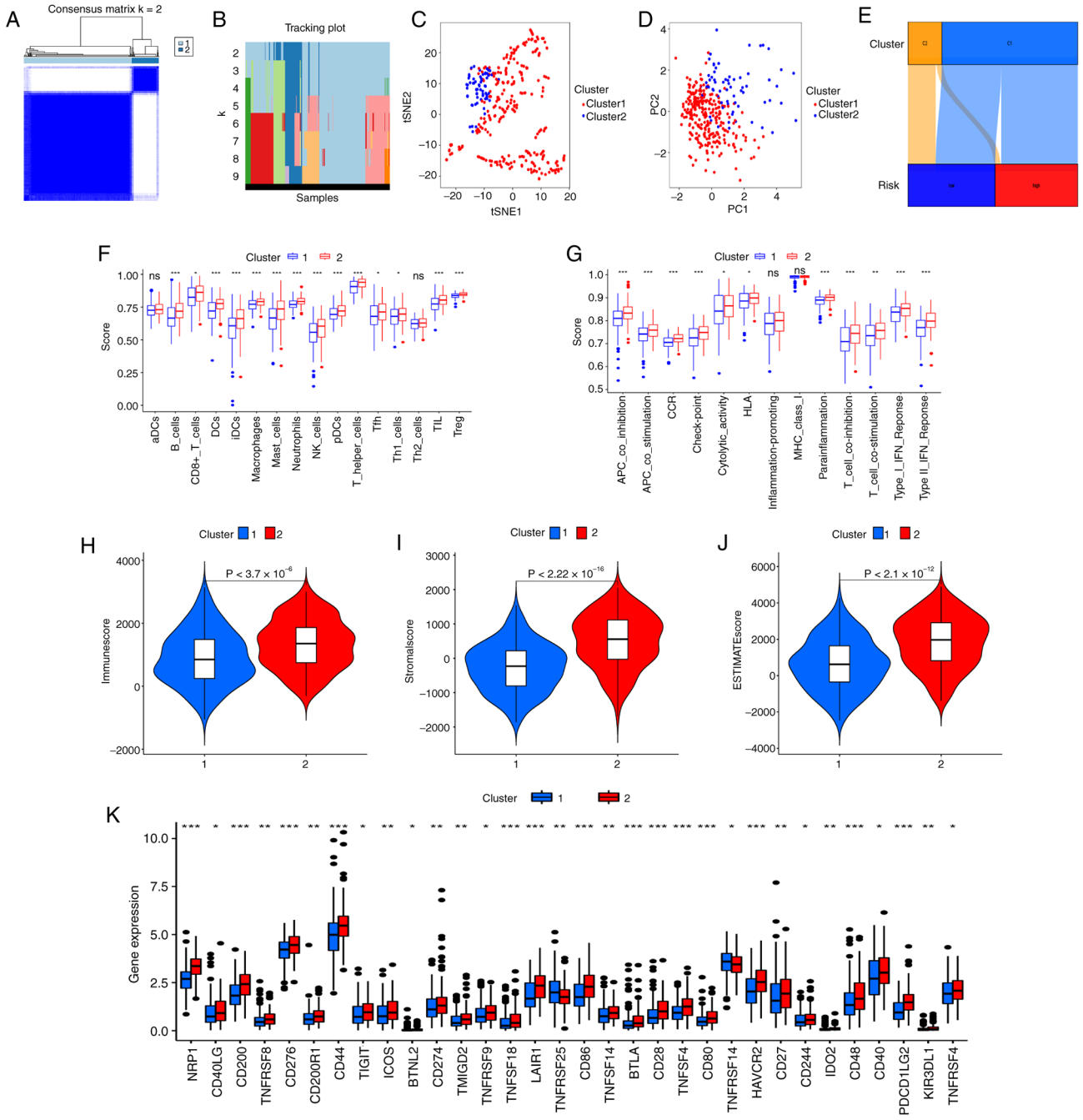


Figure 11. Hot and cold tumor identification. (A) Heatmap of matrix clustering at K=2. (B) Sample distribution for K=2-9. (C) t-SNE and (D) PC analysis for the two clusters. (E) Sankey diagram of risk and subclusters. (F) Enrichment scores of immune cells. (G) Enrichment analysis of immune-related pathways. The two clusters' (H) Immunescore, (I) Stromalscore and (J) ESTIMATEscore are compared. (K) Differences in checkpoint expression in clusters. $^{*}$P<0.05, $^{**}$P<0.01, $^{***}$P<0.001. t-SNE, t-distributed stochastic neighbor embedding; PC, principal component.

mast cells and monocytes rose with the climbing risk score. The above increased immune cells can be associated with a poorer outcome in patients with STAD. Previous studies have revealed that high density of monocytes, activated dendritic cells and resting mast cells are relatively unfavorable signals for the prognosis of patients with gastric cancer (38-40), which is consistent with the present findings. A previous study demonstrated that patients with gastric cancer had a considerable increase in neutrophil infiltration in their tumor tissues, according to flow cytometry analyses. In addition, neutrophils promote tumor progression through immunosuppressive pathways (41). Based on the analysis of drug IC50 values the present study, the model can be used as a possible predictor of drug sensitivity for chemotherapy therapies.

Tumor cells prevent immune cells from killing cancer cells by initiating immunosuppressive mechanisms, a condition that occurs mainly in hot tumors. To address this situation, emerging ICI therapies or other immunotherapies can target immune cells (mainly T cells) around tumor cells, thus triggering an immune response that kills the hot tumor (42). However, in cold tumors, the aforementioned ICI or immunotherapy is not notably effective. This is mainly due to the lack of effective mutant proteins on the cell surface of cold tumors to activate and attract

immune cells (43). STAD is a markedly gene-heterogeneous malignancy, which makes conventional clinicopathological assessment unable to reliably predict the effect of immunotherapy (44). Consensus clustering was used in the present study to divide the STAD samples into two clusters based on the SenRLs risk signature. Notably, the ESTIMATE score for Cluster 2 was significantly greater than Cluster 1, and the two clusters had a different TME. Cluster 2 is more susceptible to infiltration by immune cells, especially T cells and dendritic cells, such as Treg, Tfh, Th1 cells, iDCs, pDCs, DCs and CD8+ T cells. In addition, Cluster 2 has a greater role in controlling immune cell functions, such as T cell co-stimulation. It has been confirmed that the immune effect of the body against tumors is mainly a T cell-mediated specific cellular immune response (45). The most potent antigen-presenting cells in the organism, dendritic cells, play a notable part in the antitumor immune response (46). Immature dendritic cells *in vivo* transform and mature after uptake of foreign antigens. They then activate CD8+ T cells via major histocompatibility complex I molecules, thereby inducing an immune response (47). Compared with drug therapy, patients with tumors treated with dendritic cell vaccines as well as activated T cells after surgery have notably longer OS (48), and tumor immunotherapy based on them will likely be one of the most effective therapies (49). Notably, the present study showed that Cluster 2 had high expression levels of immunological checkpoints, including *PDCD1LG2* (also called *PD-L2*), *HAVCR2* (also called *TIM3*) and *CD274* (also called *PD-L1*). The comprehensive multi-dimensional immune characterization performed in the present study, encompassing immune cell infiltration, immune function enrichment, TME scoring and immune checkpoint expression, provides robust and consistent *in silico* evidence that the SenRLs signature can effectively distinguish hot and cold tumor phenotypes, supporting its potential value in predicting immunotherapy responsiveness. Cluster 2 exhibited a higher TME score, greater immune cell infiltration and pathway enrichment, as well as elevated expression of immune checkpoints, suggesting that it may be more sensitive to immunotherapy and thus can be defined as a hot tumor. By contrast, Cluster 1 can be classified as a cold tumor. Notably, Cluster typing based on the SenRLs risk signature can effectively discriminate between hot and cold tumors, this represents a unique advantage of the present study, as existing STAD prognostic models (whether lncRNA-based or senescence-related) fail to integrate these two dimensions to address the unmet clinical need for immunotherapy stratification (34,50,51). This capability will facilitate more accurate identification of patients who may benefit from STAD immunotherapy.

Among the five identified lncRNAs, only LINC02057 was previously linked to prognosis in lung and esophageal cancers (52,53), aligning with the present observation of its risk-associated elevation. To the best of our knowledge, the present study is the first to characterize LINC02057 as a SenRL in STAD and to explore its utility in distinguishing tumor immune phenotypes. Furthermore, the present signature represents the first model to integrate SenRLs with hot/cold tumor classification for guiding immunotherapy stratification, effectively bridging a gap in existing literature.

Due to the lack of suitable external cohorts with complete 5-year OS and lncRNA profiles, multi-model ROC validation and SHAP analysis were performed as robust validation strategies. High AUC values across multiple algorithms verified the stability of the signature. SHAP analysis revealed that AL139147.1 contributed most notably to the prognostic model, which was consistent with the results of multivariate Cox regression. This consistency confirms that the selection of key SenRLs was not arbitrary but based on their actual contributions to STAD prognosis, supporting the validity and stability of the signature. Risk-associated SenRLs exerted positive contributions, whereas protective SenRLs showed negative contributions, a pattern consistent with the risk model. These SHAP results were in line with the bioinformatic and RT-qPCR findings, further validating the accuracy of the signature and clarifying the impact of each SenRL on STAD prognosis.

The present study has several limitations. First, a cohort directly treated with immunotherapy was not included, owing to the limited availability of public STAD cohorts with documented immunotherapy administration and complete follow-up data. In future studies, clinical samples from patients with STAD receiving immunotherapy will be collected to further validate the predictive value of the SenRLs signature for immunotherapy response. Second, detailed stratified analysis of STAD subtypes was not performed due to incomplete subtype annotations in TCGA dataset. In subsequent research, complete subtype data from public databases will be integrated to validate the applicability of the SenRLs signature across different STAD subtypes. Finally, the sample size for RT-qPCR validation was relatively small, primarily due to the strict inclusion and exclusion criteria, as well as the limited availability of voluntarily enrolled cases during the study period. It is acknowledged that this small sample size may limit the statistical power of the present validation results. Consequently, future studies with larger, multicenter cohorts are warranted to further validate the expression patterns and clinical significance of these five key SenRLs.

In conclusion, based on five SenRLs (AL139147.1, LINC02057, AC093801.1, AL353804.2, AC005363.2), the present study identified a novel prognostic model of STAD. Notably, the SenRLs signature facilitates the discrimination of hot and cold tumors in STAD by identifying immune phenotypes associated with immunotherapy sensitivity. This will better screen the population for the benefits of immunotherapy and save medical resources while achieving individualized immunotherapy.

**Acknowledgements**

Not applicable.

**Funding**

The present study was supported by Xingtai Key R&D Program Project (grant no. 2025ZC072).

**Availability of data and materials**

The data generated in the present study may be requested from the corresponding author.

## Authors' contributions

FK conceived and designed the study and revised the manuscript. CH, BH, LL and XW performed the data collection, analysis and experiments. Part of the data analysis was assisted by XK, PZ and QZ. CH wrote the manuscript. FK and CH confirm the authenticity of all the raw data. All authors read and approved the final manuscript.

## Ethics approval and consent to participate

The present study was approved by the Ethics Committee of Xingtai People's Hospital (approval no. 2025-048), and all studies were conducted in accordance with relevant guidelines. All patients agreed and signed the informed consent form. The study was conducted in accordance with The Declaration of Helsinki.

## Patient consent for publication

Not applicable.

## Competing interests

The authors declare that they have no competing interests.

## References


1. Bray F, Laversanne M, Sung H, Ferlay J, Siegel RL, Soerjomataram I, Jemal A and Torre LA: Global cancer statistics 2022: GLOBOCAN estimates of incidence and mortality worldwide for 36 cancers in 185 countries. CA Cancer J Clin 74: 229-263, 2024.
2. Ajani JA, D'Amico TA, Bentrem DJ, Corvera CU, Das P, Enzinger PC, Enzler T, Gerdes H, Gibson MK, Grierson P, *et al*: Gastric cancer, version 2.2025, NCCN clinical practice guidelines in oncology. J Natl Compr Canc Netw 23: 169-191, 2025.
3. Sundar R, Nakayama I, Markar SR, Shitara K, van Laarhoven HWM, Janjigian YY and Smyth EC: Gastric cancer. Lancet 405: 2087-2102, 2025.
4. Christodoulidis G, Koumarelas KE and Kouliou MN: Revolutionizing gastric cancer treatment: The potential of immunotherapy. World J Gastroenterol 30: 286-289, 2024.
5. Kanaji S, Urakawa N, Harada H, Ikeda T, Koterazawa Y, Aoki T, Sawada R, Otowa Y, Goto H, Hasegawa H, *et al*: Multidisciplinary treatment for advanced gastric cancer. Int J Clin Oncol 30: 1268-1275, 2025.
6. Luo D, Liu Y, Lu Z and Huang L: Targeted therapy and immunotherapy for gastric cancer: Rational strategies, novel advancements, challenges, and future perspectives. Mol Med 31: 52, 2025.
7. Liu YT, Wang YL, Wang S, Li JJ, He W, Fan XJ and Wan XB: Turning cold tumors into hot tumors to ignite immunotherapy. Mol Cancer 24: 254, 2025.
8. Kong X, Ou S, Wei Z, Ye X, Chen S, Shi X and Zhang R: Transforming the 'cold' tumors to 'hot' tumors: Strategies for immune activation. Biochem Pharmacol 241: 117194, 2025.
9. Wu B, Zhang B, Li B, Wu H and Jiang M: Cold and hot tumors: From molecular mechanisms to targeted therapy. Signal Transduct Target Ther 9: 274, 2024.
10. Sun F, Gao X, Wang W, Zhao X, Zhang J and Zhu Y: Predictive biomarkers in the era of immunotherapy for gastric cancer: Current achievements and future perspectives. Front Immunol 16: 1599908, 2025.
11. Yasuda T and Wang YA: Gastric cancer immunosuppressive microenvironment heterogeneity: Implications for therapy development. Trends Cancer 10: 627-642, 2024.
12. Sun F, Gao X, Li T, Zhao X and Zhu Y: Tumor immune microenvironment remodeling after neoadjuvant therapy in gastric cancer: Update and new challenges. Biochim Biophys Acta Rev Cancer 1880: 189350, 2025.
13. Marin I, Boix O, Garcia-Garijo A, Sirois I, Caballe A, Zarzuela E, Ruano I, Attolini CS, Prats N, Lopez-Dominguez JA, *et al*: Cellular senescence is immunogenic and promotes antitumor immunity. Cancer Discov 13: 410-431, 2023.
14. Yasuda T, Baba H and Ishimoto T: Cellular senescence in the tumor microenvironment and context-specific cancer treatment strategies. FEBS J 290: 1290-1302, 2023.
15. Fakhri S, Zachariah Moradi S, DeLiberto LK and Bishayee A: Cellular senescence signaling in cancer: A novel therapeutic target to combat human malignancies. Biochem Pharmacol 199: 114989, 2022.
16. Chen LL and Kim VN: Small and long non-coding RNAs: Past, present, and future. Cell 187: 6451-6485, 2024.
17. Kadian LK, Verma D, Lohani N, Yadav R, Ranga S, Gulshan G, Pal S, Kumari K and Chauhan SS: Long non-coding RNAs in cancer: Multifaceted roles and potential targets for immunotherapy. Mol Cell Biochem 479: 3229-3254, 2024.
18. Jin P, Duan X, Li L, Zhou P, Zou CG and Xie K: Cellular senescence in cancer: Molecular mechanisms and therapeutic targets. MedComm (2020) 5: e542, 2024.
19. Chatterjee M and Viswanathan P: Long noncoding RNAs in the regulation of p53-mediated apoptosis in human cancers. Cell Biol Int 45: 1364-1382, 2021.
20. Tavares E Silva J, Pessoa J, Nóbrega-Pereira S and Bernardes de Jesus B: The impact of long noncoding RNAs in tissue regeneration and senescence. Cells 13: 119, 2024.
21. Sang B, Zhang YY, Guo ST, Kong LF, Cheng Q, Liu GZ, Thorne RF, Zhang XD, Jin L and Wu M: Dual functions for OVAAL in initiation of RAF/MEK/ERK prosurvival signals and evasion of p27-mediated cellular senescence. Proc Natl Acad Sci USA 115: E11661-E11670, 2018.
22. Sang Y, Tang J, Li S, Li J, Zhang Y, Chen L, Han L and Wang X: LncRNA PANDAR regulates the G1/S transition of breast cancer cells by suppressing p16(INK4A) expression. Sci Rep 6: 22366, 2016.
23. Fan SB, Xie XF, Wei W and Hua T: Senescence-Related LncRNAs: Pioneering indicators for ovarian cancer outcomes. Phenomics 4: 379-393, 2024.
24. Cao L, Chen F, Xu L, Zeng J, Wang Y, Zhang S, Ba Y and Zhang H: Prognostic cellular senescence-related lncRNAs patterns to predict clinical outcome and immune response in colon cancer. Front Immunol 15: 1450135, 2024.
25. Chen L, Lin J, Wen Y, Lan B, Xiong J, Fu Y, Chen Y and Chen CB: A senescence-related lncRNA signature predicts prognosis and reflects immune landscape in HNSCC. Oral Oncol 149: 106659, 2024.
26. Schober P, Boer C and Schwarte LA: Correlation coefficients: Appropriate use and interpretation. Anesth Analg 126: 1763-1768, 2018.
27. Lauren P: The two histological main types of gastric carcinoma: Diffuse and so-called intestinal-type carcinoma. Acta Pathol Microbiol Scand 64: 31-49, 1965.
28. Nagtegaal ID, Odze RD, Klimstra D, Paradis V, Rugge M, Schirmacher P, Washington KM, Carneiro F and Cree IA; WHO Classification of Tumours Editorial Board: The 2019 WHO classification of tumours of the digestive system. Histopathology 76: 182-188, 2020.
29. Livak KJ and Schmittgen TD: Analysis of relative gene expression data using real-time quantitative PCR and the 2(-Delta Delta C(T)) method. Methods 25: 402-408, 2001.
30. Marin-Acevedo JA, Kimbrough EO and Lou Y: Next generation of immune checkpoint inhibitors and beyond. J Hematol Oncol 14: 45, 2021.
31. Binnewies M, Roberts EW, Kersten K, Chan V, Fearon DF, Merad M, Coussens LM, Gabrilovich DI, Ostrand-Rosenberg S, Hedrick CC, *et al*: Understanding the tumor immune microenvironment (TIME) for effective therapy. Nat Med 24: 541-550, 2018.
32. Roger L, Tomas F and Gire V: Mechanisms and regulation of cellular senescence. Int J Mol Sci 22: 13173, 2021.
33. Tesfaye E, Martinez-Terroba E, Bendor J, Winkler L, Olivero C, Chen K, Feldser DM, Zamudio JR and Dimitrova N: The p53 transcriptional response across tumor types reveals core and senescence-specific signatures modulated by long noncoding RNAs. Proc Natl Acad Sci USA 118: e2025539118, 2021.
34. Zhou L, Niu Z, Wang Y, Zheng Y, Zhu Y, Wang C, Gao X, Gao L, Zhang W, Zhang K, *et al*: Senescence as a dictator of patient outcomes and therapeutic efficacies in human gastric cancer. Cell Death Discov 8: 13, 2022.

35. Lv MY, Cai D, Li CH, Wang Y, Zhang X, Liu H, Chen J, Wu Q and Zhang Z: Senescence-based colorectal cancer subtyping reveals distinct molecular characteristics and therapeutic strategies. MedComm (2020) 4: e333, 2023.
36. Wu Y, Xu R, Wang J and Luo Z: Precision molecular insights for prostate cancer prognosis: Tumor immune microenvironment and cell death analysis of senescence-related genes by machine learning and single-cell analysis. Discov Oncol 15: 487, 2024.
37. Zeng D, Li M, Zhou R, Zhang J, Sun H, Shi M, Bin J, Liao Y, Rao J and Liao W: Tumor microenvironment characterization in gastric cancer identifies prognostic and immunotherapeutically relevant gene signatures. Cancer Immunol Res 7: 737-750, 2019.
38. Urakawa S, Yamasaki M, Goto K, Haruna M, Hirata M, Morimoto-Okazawa A, Kawashima A, Iwahori K, Makino T, Kurokawa Y, *et al*: Peri-operative monocyte count is a marker of poor prognosis in gastric cancer: Increased monocytes are a characteristic of myeloid-derived suppressor cells. Cancer Immunol Immunother 68: 1341-1350, 2019.
39. Yang X, Lei P, Huang L, Tang X, Wei B and Wei H: Prognostic value of LRRC4C in colon and gastric cancers correlates with tumour microenvironment immunity. Int J Biol Sci 17: 1413-1427, 2021.
40. Zhao Y, Hu S, Zhang J, Guo Y, Li Y, Wu L, Zhang L and Wang X: Glucoside xylosyltransferase 2 as a diagnostic and prognostic marker in gastric cancer via comprehensive analysis. Bioengineered 12: 5641-5654, 2021.
41. Wang TT, Zhao YL, Peng LS, Chen N, Chen W, Lv YP, Liu FY, Zhang JY, Cheng P, Teng YS, *et al*: Tumour-activated neutrophils in gastric cancer foster immune suppression and disease progression through GM-CSF-PD-L1 pathway. Gut 66: 1900-1911, 2017.
42. Duan Q, Zhang H, Zheng J and Zhang L: Turning cold into hot: Firing up the tumor microenvironment. Trends Cancer 6: 605-618, 2020.
43. Galon J and Bruni D: Approaches to treat immune hot, altered and cold tumours with combination immunotherapies. Nat Rev Drug Discov 18: 197-218, 2019.
44. Chen Y, Sun Z, Chen W, Liu C, Chai R, Ding J, Liu W, Feng X, Zhou J, Shen X, *et al*: The immune subtypes and landscape of gastric cancer and to predict based on the whole-slide images using deep learning. Front Immunol 12: 685992, 2021.
45. Chopp L, Redmond C, O'Shea JJ and Schwartz DM: From thymus to tissues and tumors: A review of T-cell biology. J Allergy Clin Immunol 151: 81-97, 2023.
46. Heras-Murillo I, Adán-Barrientos I, Galán M, Wculek SK and Sancho D: Dendritic cells as orchestrators of anticancer immunity and immunotherapy. Nat Rev Clin Oncol 21: 257-277, 2024.
47. MacNabb BW, Chen X, Tumuluru S, Godfrey J, Kasal DN, Yu J, Jongsma MLM, Spaapen RM, Kline DE and Kline J: Dendritic cells can prime anti-tumor CD8+ T cell responses through major histocompatibility complex cross-dressing. Immunity 55: 982-997, 2022.
48. Shimizu K, Kotera Y, Aruga A, Takeshita N, Katagiri S, Ariizumi S, Takahashi Y, Yoshitoshi K, Takasaki K and Yamamoto M: Postoperative dendritic cell vaccine plus activated T-cell transfer improves the survival of patients with invasive hepatocellular carcinoma. Hum Vaccin Immunother 10: 970-976, 2014.
49. Fu C, Ma T, Zhou L, Mi QS and Jiang A: Dendritic cell-based vaccines against cancer: Challenges, advances and future opportunities. Immunol Invest 51: 2133-2158, 2022.
50. He J, Fu Z, Zou B, Lei X, Lei L, Yang Q and Li G: Identification the cellular senescence associated lncRNA LINC01579 in gastric cancer. J Cell Mol Med 29: e70360, 2025.
51. Ding X, Zhang Y and You S: A novel prognostic model based on telomere-related lncRNAs in gastric cancer. Transl Cancer Res 13: 4608-4624, 2024.
52. Lei Q, Fan BF, Zhu XR, Cui BW, Kong JX, Ma ZR, Xie XQ and Wang WW: Immune infiltration and drug treatment response of angiogenesis-related LncRNA in lung adenocarcinoma. Medicine (Baltimore) 104: e42958, 2025.
53. Ma Y, Sun Y, Zhao X, Li J, Fu X, Gong T and Zhang X: Identification of m5C-related lncRNAs signature to predict prognosis and therapeutic responses in esophageal squamous cell carcinoma patients Sci Rep 13: 14499, 2023.